Electronic Supplementary Material (ESI) for Lab on a Chip.

Supplemental Materials for:

Dissolution-After-Precipitation (DAP): A Simple Microfluidic Approach for Studying Carbonate Rock Dissolution and Multiphase Reactive Transport Mechanisms

Jianping Xu [1,2] and Matthew T. Balhoff [1,2]

[1] Hildebrand Department of Petroleum and Geosystems Engineering, The University of Texas at Austin, Austin, Texas 78712, USA

[2] Center for Subsurface Energy and the Environment, The University of Texas at Austin, Austin, Texas 78712, USA

1. Measurement of diffusive mixing band width

Images from the color mixing experiments can be analyzed to obtain width of diffusive mixing band. An Otsu thresholding method is used to binarize the image in ImageJ, and the binarized version could be used to measure band width. The binarized images of Fig. 4 are shown in Fig. S1.

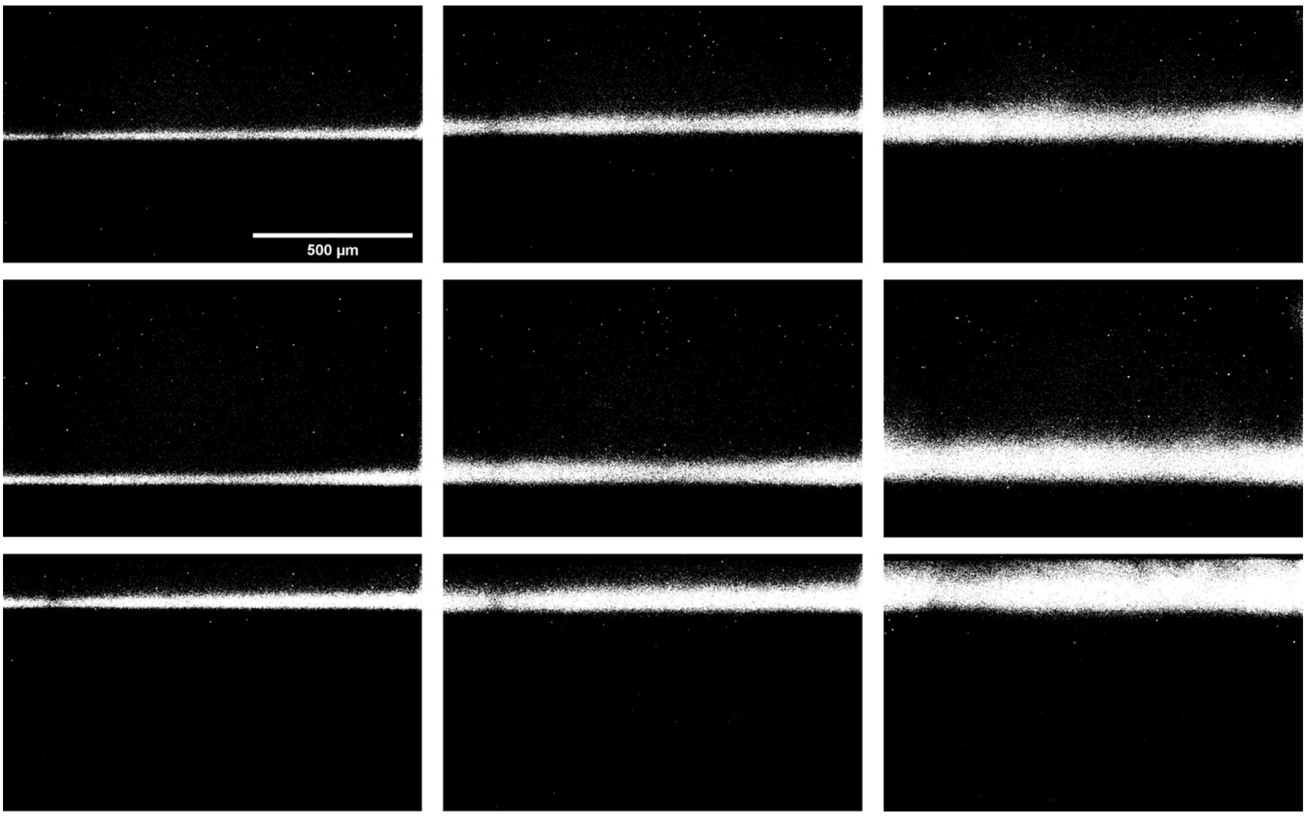

Figure S1. Binarized version of Fig. 4.

As shown in Fig. S1, there is non-negligible noise in the binarized images. To measure effective width of the band, we first measure the total area of the white pixel region, then divide it by the length of the image. This yields the width of a rectangle that has the same area as the white band in Fig. S1. The results are shown in Tab. S1.

Table S1. Measurements of effective width of the diffusive mixing bands in Fig. S1

Flow rate pair (μL/h, μL/h)	Location	Effective band width (μm)
(20, 20)	Upstream	24
(20, 20)	Midstream	49
(20, 20)	Downstream	98
(20, 5)	Upstream	31
(20, 5)	Midstream	64
(20, 5)	Downstream	139
(5, 20)	Upstream	42
(5, 20)	Midstream	74
(5, 20)	Downstream	135

2. Precipitation profile along the channel

In this section we present one experimental example of an increasingly more homogeneous precipitation profile from upstream to downstream of the channel. The snapshots from the experiment are shown in Fig. S2.

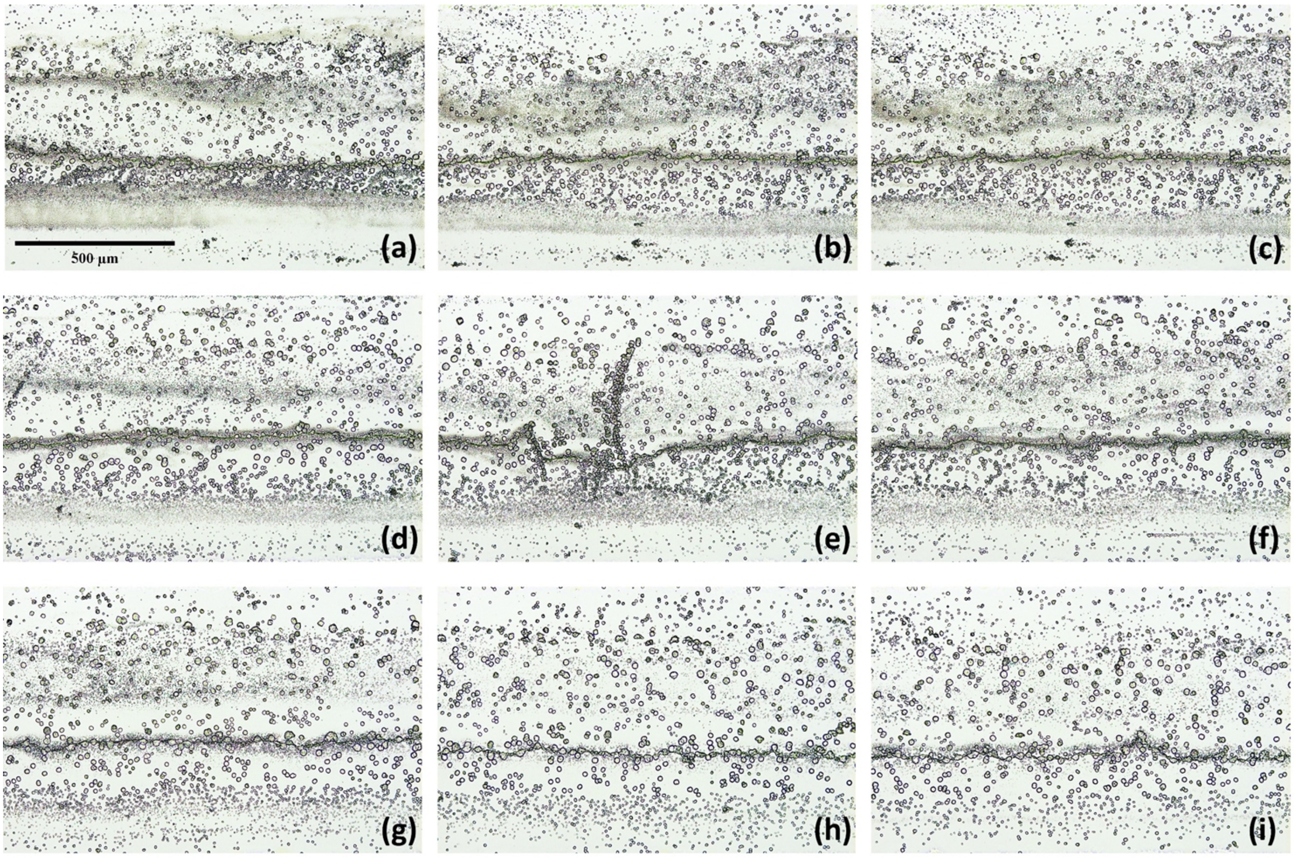

Figure S2. Experimental snapshots of the increasingly more homogeneous precipitation profile from upstream to downstream. The distance of the observation window from the junction increases from (a) to (i).

From the figure, we see that at the upstream, there are several stripes of high density of grains aggregation, signaling the historical presence of multiple diffusive mixing bands. Consequently, the structure of the porous medium is heterogeneous across the transverse direction. At the last panel (i), there is only one thin line of grain aggregation, and the overall distribution of grains is mostly uniform, although there is still difference between individual crystal grains' size.

3. Arithmetic mean and weighted mean

In the paper we have used arithmetic mean ($\bar{S}^H$) of S_i^H to calculate the characteristic length scale d. One alternative is the weighted mean, which could be expressed as

$$\bar{S}^H|_w = \sum_{i=1}^{N} f(S_i^H) S_i^H$$

where $f(S_i^H)$ is the probability to have an area of S_i^H, and $f(\cdot)$ is the probability density function of the area. The histogram of the area, such as shown in Fig. 6, is a natural representation of $f(\cdot)$ when normalized. We constructed $f(\cdot)$ from S_i^H's data using a logarithmic binning method[1]. We chose logarithmic binning over binning in linear scale because the sizes of areas cover several orders of magnitude, which will introduce massive noise in the latter. The computed probability density functions for initial state of Exp 1-7 are shown in Fig. S3.

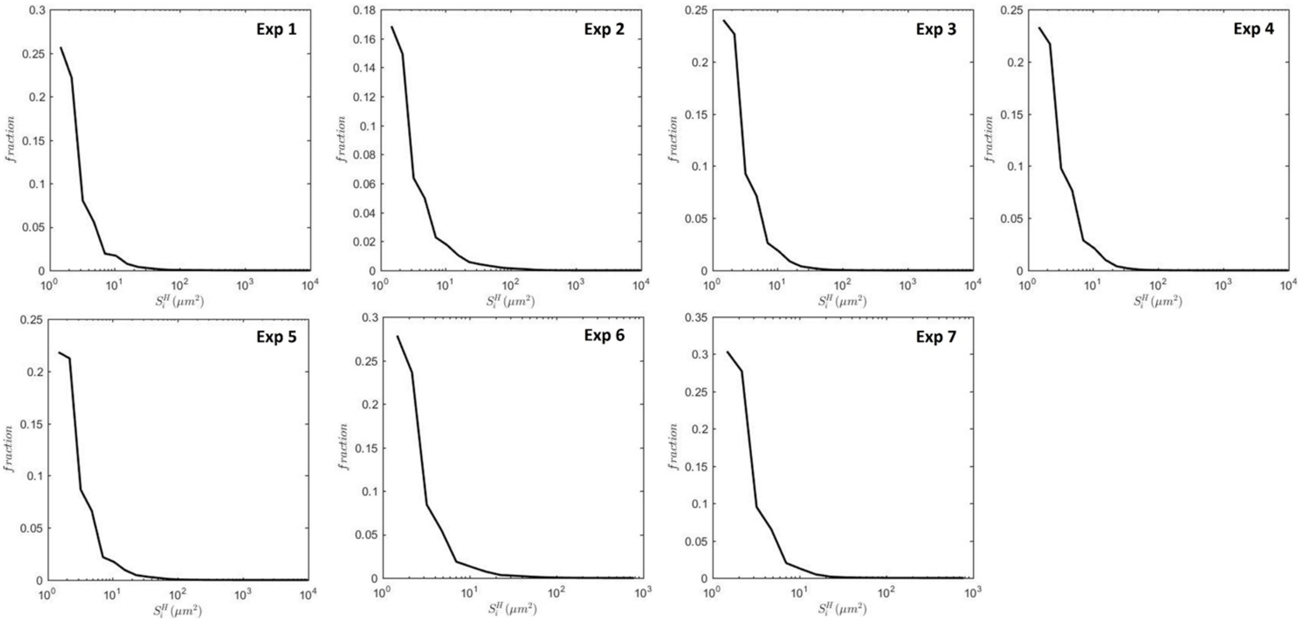

Figure S3. The probability density functions of particles sizes in Exp 1-7.

Using the probability density functions, we can calculate $\bar{S}^H|_w$ and compare the values to the arithmetic means.

The normalized histograms assign weights based on numbers/populations. The other way of assigning weights is by particle's areas. The following equation calculates weighted mean based on areas:

$$\bar{S}^H|_w = \frac{\sum_{i=1}^{N} S_i^H S_i^H}{\sum_{i=1}^{N} S_i^H}$$

Under this definition, $f(S_i^H) = \frac{S_i^H}{\sum_{i=1}^{N} S_i^H}$. We calculate the weighted means also based on this definition. The results are summarized in Tab. S2.

Table S2. Comparison between characteristic horizontal areas of grains using arithmetic mean and weighted mean

Experiment # Exp ()	$\bar{S}^H$ (μm^2), arithmetic mean	$\bar{S}^H\vert_w$ (μm^2), weighted by numbers	$\bar{S}^H\vert_w$ (μm^2), weighted by areas
1	26.70	2.29	5469
2	52.84	2.56	13619
3	17.05	2.34	11487
4	10.78	2.36	2164
5	44.36	2.41	69034
6	10.10	2.22	118
7	4.96	1.14	95

Data in Tab. S2 show that using weights based on particle numbers and particle areas have produced starkly different results. As elaborated in section 2.4 of the paper, the particle statistics is heavily biased such that large numbers of small particles only account for small fraction of total areas in the system, while small numbers of larger particles possess large fraction of total areas. Therefore, when weighted by numbers, the mean would be dominated by the small particles. When weighted by areas, the mean would be dominated by few extremely large particles due to the square operation in the numerator. The arithmetic means situate between these two extremes and seem to better describe a combined effect of small and large particles. Therefore, we used the arithmetic mean in the paper.

4. Smallest particles in the histogram

In Fig. 6 of the paper, the smallest particles on the left end of the histogram are about 1 μm^2, which is close to the resolution of the image (0.8892 μm^2/pixel area, or 0.943 μm/pixel length). In this section we show a close-up comparison of these smallest particles in the raw image and binarized image from Fig. 6. The comparison is shown in Fig. S4.

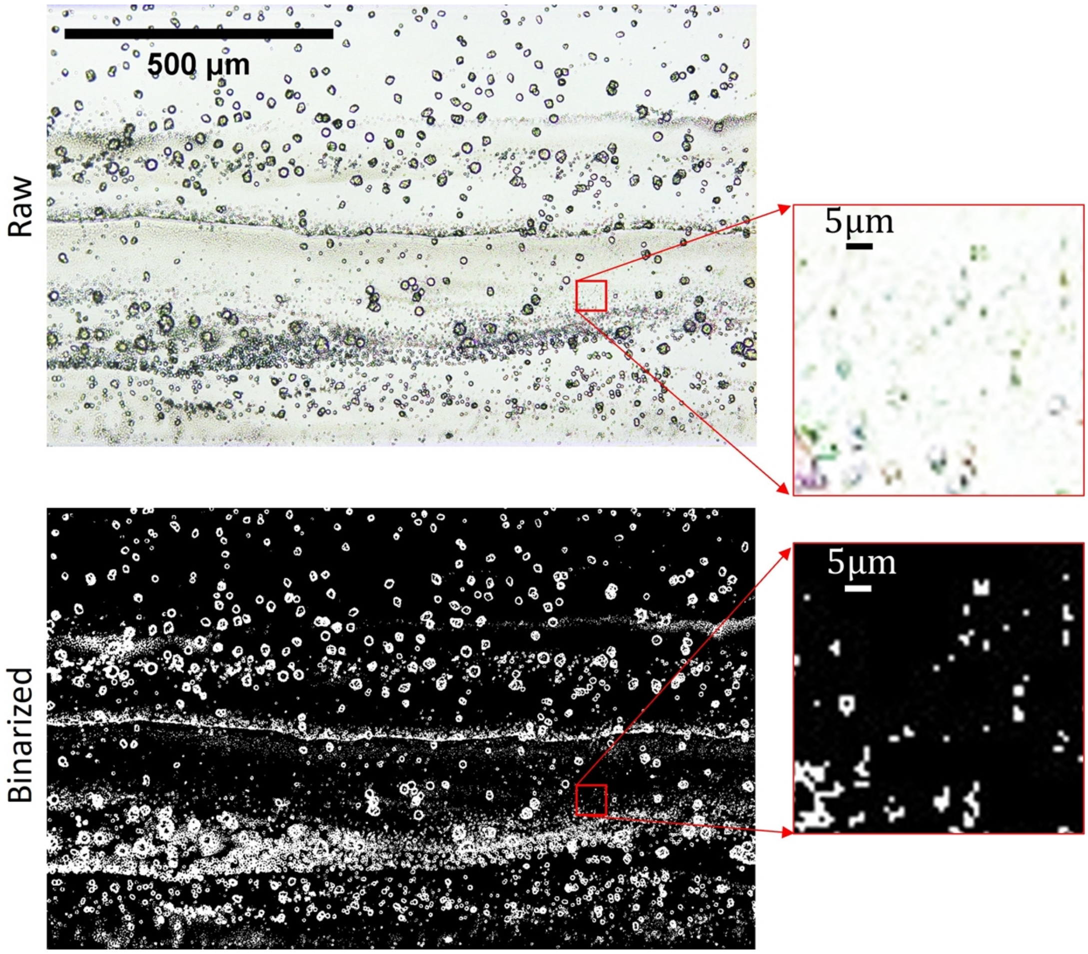

Figure S4. Comparison between smallest particles in the raw image and binarized image.

The zoomed in window contains several particles that are close to the image resolution. We see that the binarized image matches well with the raw image in terms of identifying these smallest particles. We conclude that these smallest particles are not noises in image analysis.

5. Wettability characterization

The wettability of the solid grains is characterized using contact angle between acid and the grain. We collected 15 instances of acid-grain contacts in Exp 6, from which 24 measurements of contact angle could be made. These instances are presented in Fig. S5.

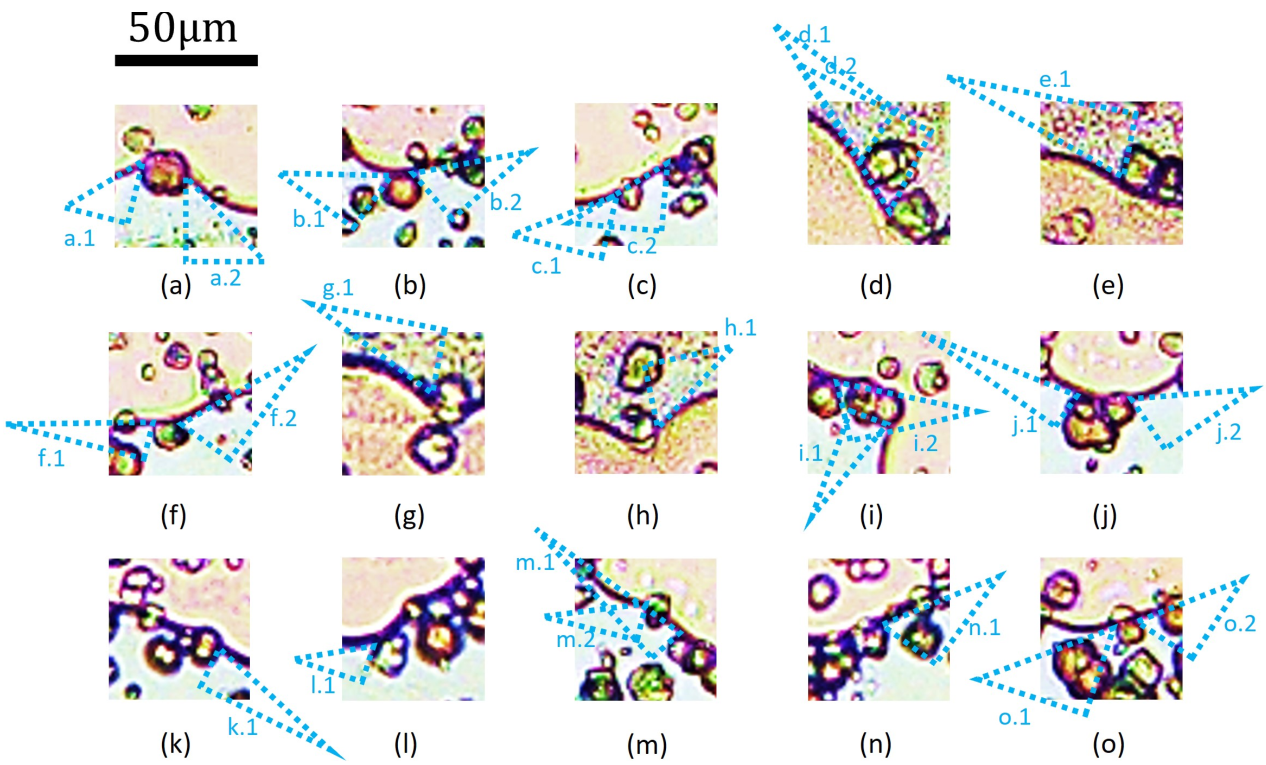

Figure S5. The measurements of acid contact angles. The angle is calculated from inverse tangent of the ratio of the two right-angle sides.

The contact angle is calculated from the inverse tangent of the ratio of the two right-angle sides of the measuring triangle. Results of the acid contact angles are summarized in Tab. S3.

Table S3. Results of acid contact angle measurements

Angle #	Acid contact angle (°)
a.1	45.0
a.2	42.5
b.1	55.3
b.2	59.2
c.1	55.3
c.2	53.8
d.1	68.6
d.2	59.2
e.1	71.6
f.1	75.3
f.2	65.3
g.1	64.7
h.1	54.8
i.1	70.8
i.2	65.0
j.1	77.0

j.2	60.5
k.1	73.5
l.1	62.9
m.1	77.8
m.2	68.7
n.1	58.3
o.1	51.0
o.2	54.6

Data showing in Tab. S3 indicate that the wettability of the medium is not uniformly distributed in space. In different regions of the porous medium, the contact angle varies. The data range from 45.0° to 77.8°, with an average contact angle of 62.1°. Thus the medium is water-wet, but not strongly water-wet.

6. Calculations of acid resident times

The resident time of acid in the domain of interest is calculated by the interstitial velocities of acid (v) and the length of the domain (l_{win}, defined in the paper) as follows,

$$\tau = \frac{l_{win}}{v}$$

where $v = \frac{q}{A_c\phi}$ is the interstitial velocity.

The results for resident times of Exp 1-7 are summarized in Tab. S4.

Table S4. Resident times of acid

Experiment # Exp ()	Resident time (s)
1	0.99
2	270.71
3	1.78
4	0.53
5	0.14
6	12.81
7	19.02

Longer resident time corresponds to slower acid delivery. When the acid spends longer time in the domain of interest, it also means fresh acid take longer time to arrive. In such a way, the dissolution could be slow since local acidity can be exhausted without a timely replenishment. For example, in the compact dissolution, the resident time is the highest, and it is also the slowest one.

7. Characteristic length of pore spaces

In Eq. (4) we have used the characteristic grain size d to construct the Peclet number. One may also use the characteristic length of the pore spaces. Here we denote this length as D.

To generate the characteristic length of the pore spaces, a similar workflow to Fig. 6 would work. Instead, we need to reverse the background of the image such that particles becomes “pores” and pores spaces becomes “particles”. After this, the Particle Analysis procedure could give the mean area of pore “particles”, with which we can calculate D. Here, using Exp 5 as example.

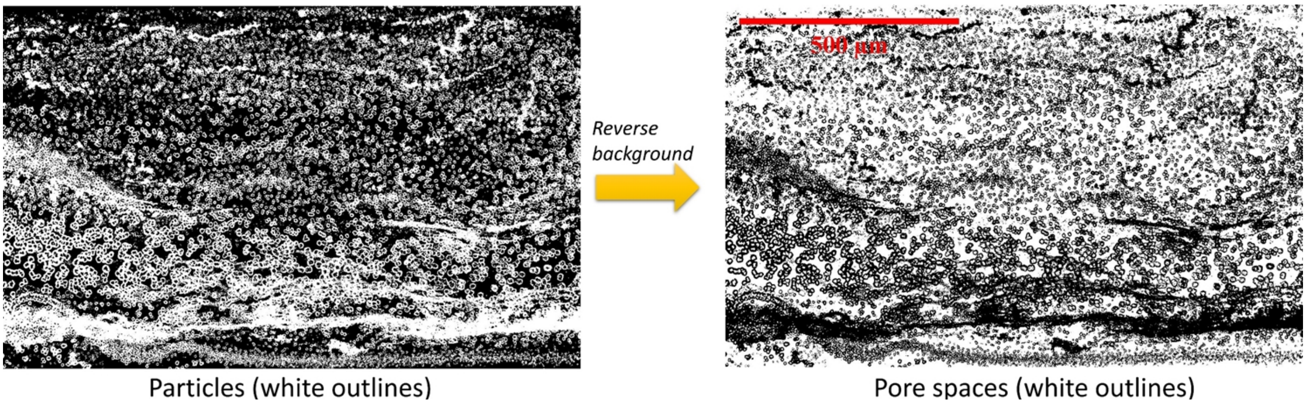

Figure S6. Background reverse for the size analysis of pore spaces. Scale bar is 500 microns.

After reversing the background, pore spaces become the “particles” and its statistics can be computed. After obtaining the mean areas, we can calculate the length by square root of the data. Results of *D* with its comparison to *d* are shown in Tab. S5.

Table S5. Comparison of characteristic lengths of solid grains and pore spaces

Experiment # Exp ()	Grain length (µm)	Pore space length (µm)
1	5.17	18.11
2	7.27	14.34

3	4.13	21.58
4	3.28	23.95
5	6.66	7.98

Data in the table show that the characteristic lengths of pore spaces are all larger than the grains. This is reasonable since the porosities of these five media are relatively high (Tab. 2 in the paper). Exp 5 has the lowest porosity, and the two lengths are close. One may also use these pore spaces lengths to construct Peclet number, but the resulting values could be different.

8. Caption for supplemental video 1.

This video records the retreat of the central CO_2 ganglia due to the expansion of the north and south wormholes. The video starts from Fig. 13(m) and stops at Fig. 13(p).

9. Caption for supplemental video 2.

This video captures the escape of the trapped CO_2 gas ganglia from the north wormhole to the south's much wider wormhole in Exp 7S. Such gas redistribution causes a counterflow of CO_2 (opposite to the flow of acid) in the north wormhole.

10. Caption for supplemental video 3.

This video captures the inflection of an advancing cone by dense particle zones in Exp 3S.2. The dense particle zone (which is harder to dissolve) causes the cone to change its direction of advancement. This shows that the impact of heterogeneity on channeling behaviors is significant. There is an active interplay between channeling and porous medium heterogeneity.

11. References

1. Newman MEJ. Power laws, Pareto distributions and Zipf's law. *Contemporary Physics*. 2005;46(5):323-351.